Chinese Physics Letters

PAPER

Electronic Structure of the Weak Topological Insulator Candidate Zintl $Ba_3Cd_2Sb_4$

To cite this article: Jierui Huang *et al* 2023 *Chinese Phys. Lett.* **40** 047101

Electronic Structure of the Weak Topological Insulator Candidate Zintl $Ba_3Cd_2Sb_4$

Jierui Huang(黄杰瑞)[1,2†], Tan Zhang(张坦)[1†], Sheng Xu(徐升)[3,4†], Zhicheng Rao(饶志成)[1,2], Jiajun Li(李佳俊)[1,2], Junde Liu(刘俊德)[1,2], Shunye Gao(高顺业)[1,2], Yaobo Huang(黄耀波)[5], Wenliang Zhu(朱文亮)[6], Tianlong Xia(夏天龙)[3,4*], Hongming Weng(翁红明)[1,2,7,8*], and Tian Qian(钱天)[1,7*]

[1]*Beijing National Laboratory for Condensed Matter Physics, Institute of Physics, Chinese Academy of Sciences, Beijing 100190, China*
[2]*University of Chinese Academy of Sciences, Beijing 100049, China*
[3]*Department of Physics, Renmin University of China, Beijing 100872, China*
[4]*Beijing Key Laboratory of Opto-electronic Functional Materials & Micro-nano Devices, Renmin University of China, Beijing 100872, China*
[5]*Shanghai Synchrotron Radiation Facility, Shanghai Advanced Research Institute, Chinese Academy of Sciences, Shanghai 201204, China*
[6]*School of Physics and Information Technology, Shaanxi Normal University, Xi'an 710119, China*
[7]*Songshan Lake Materials Laboratory, Dongguan 523808, China*
[8]*CAS Center for Excellence in Topological Quantum Computation, University of Chinese Academy of Sciences, Beijing 100190, China*

(Received 2 February 2023; accepted manuscript online 1 March 2023)

One of the greatest triumph of condensed matter physics in the past ten years is the classification of materials by the principle of topology. The existence of topological protected dissipationless surface state makes topological insulators great potential for applications and hotly studied. However, compared with the prosperity of strong topological insulators, theoretical predicted candidate materials and experimental confirmation of weak topological insulators (WTIs) are both extremely rare. By combining systematic first-principles calculation and angle-resolved photoemission spectroscopy measurements, we have studied the electronic structure of the dark surface of the WTI candidate Zintl $Ba_3Cd_2Sb_4$ and another related material $Ba_3Cd_2As_4$. The existence of two Dirac surface states on specific side surfaces predicted by theoretical calculations and the observed two band inversions in the Brillouin zone give strong evidence to prove that the $Ba_3Cd_2Sb_4$ is a WTI. The spectroscopic characterization of this Zintl $Ba_3Cd_2N_4$ ($N =$ As and Sb) family materials will facilitate applications of their novel topological properties.

DOI: 10.1088/0256-307X/40/4/047101

In the past 40 years, we have witnessed the opening of a new era of condensed-matter physics: topological quantum matter. From quantum Hall effect to multifarious topological insulators (TIs) and topological semimetals, the robust spin polarized topological edge states stemming from "bulk edge correspondence" make topological materials particularly interesting and promising for applications. Among them, the Fermi level is pinned to the bulk band gap in strictly stoichiometric TIs, which makes surface Dirac fermions naturally dominate the transport behavior. Therefore, TIs are more promising in practical than topological semimetals. Three-dimensional (3D) TIs are characterized by a set of four topological indices, namely, ν_0; (ν_1, ν_2, ν_3) with $\nu_i = \{0, 1\}$. If $\nu_0 = 1$, the system is called a strong TI and has robust two-dimensional (2D) metallic surface states (SSs) on all surfaces. The perfect backscattering is prohibited by the spin-momentum locked Dirac cones dispersion. If $\nu_0 = 0$ and any other $\nu_i \neq 0$, the system is called a weak topological insulator (WTI) with robust metallic SSs on particular side surfaces but not all surfaces.[1,2] WTIs can be regarded as 3D stacking of 2D quantum spin Hall insulators,[3,4] due to the weak interlayer coupling, WTIs generally yield topological SSs with quasi-1D dispersion on side surfaces. This could strictly prohibit even general scattering off 180° to establish dissipationless spin current.[5] This advantage makes WTIs attract much attention in terms of their applications.

A WTI manifests itself by the even number of Dirac SSs on certain surfaces and even times of band inversions in the Brillouin zone.[6,7] Since multiple band inversions are required, the WTI candidate materials predicted by theoretical calculations are rare.[8–15] Not only that, experimental verification of a WTI is also extremely difficult.[16–20] The stacking structure brings it inherent

†These authors contributed equally to this work.
*Corresponding authors. Email: tlxia@ruc.edu.cn; hmweng@iphy.ac.cn; tqian@iphy.ac.cn

obstacle to cleave the side surface for experimental characterizing, such as the case in $Bi_{14}Rh_3I_9$, which is predicted to be a WTI with $\mathbb{Z}_2 = (0;001)$, while the natural cleaving plane is (001), which is a topologically dark surface without topological SSs.[9,20] Even with the help of the recent development of nano angle-resolved photoemission spectroscopy (ARPES) techniques, only a few materials have been verified as WTIs.[5,21] Until recently, the discovery of triclinic WTI $RhBi_2$ with topological SSs on the natural cleaving surface has been reported. However, this material suffers from intrinsic defects that cause self-doping, which moves the Fermi level into the bulk bands.[14] More ideal WTI materials are urgently needed to be explored.

In this Letter, by combining first-principles calculations and ARPES experiments, we reveal the electronic structure of dark surface of the WTI candidate $Ba_3Cd_2Sb_4$ and trivial semiconductor $Ba_3Cd_2As_4$. We confirm the absence of topological SSs on the dark surface by careful SSs calculations, which is an important characteristic of WTIs. The experimental measured 3D Fermi surfaces (FS) and band structures along the high symmetry lines of $Ba_3Cd_2Sb_4$ show great consistence with the Heyd–Scuseria–Ernzerhof (HSE06) calculations. The existence of two Dirac topological SSs on the (010) plane predicted by our SSs calculations and the observed two band inversions in the Brillouin zone give strong evidence for $Ba_3Cd_2Sb_4$ being a WTI. Compared with $Ba_3Cd_2Sb_4$, no band inversion is observed in $Ba_3Cd_2As_4$, which indicates $Ba_3Cd_2As_4$ to be a trivial semiconductor. Continuous topological phase transition can be achieved by chemical doping or external stressing. The easily controllable topological properties make $Ba_3Cd_2N_4$ (N = Sb and As) family materials worthy of further in-depth study and promising for applications.

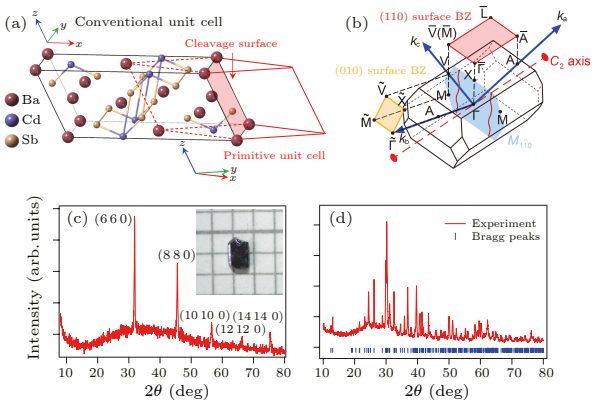

Fig. 1. (a) Crystal structure of $Ba_3Cd_2Sb_4$. The natural cleavage surface (110) is labeled by the red shaded area. (b) Three-dimensional Brillouin zone of $Ba_3Cd_2Sb_4$ and its surface projections with high-symmetry points indicated. Single-crystal (c) and powder (d) x-ray diffraction data of $Ba_3Cd_2Sb_4$ single crystal. The inset of (c) exhibits a picture of the typical grown $Ba_3Cd_2Sb_4$ single crystal with (110) surface. The blue vertical bars in (d) represent the expected Bragg reflection positions of $Ba_3Cd_2Sb_4$.

The Zintl compounds $Ba_3Cd_2Sb_4$ and $Ba_3Cd_2As_4$ crystallize with the monoclinic space group $C2/m$ (No. 12), conventional unit cell parameters $a = 17.835(2)$ Å, $b = 4.8675(5)$ Å, $c = 7.6837(7)$ Å, and $\beta = 112.214(1)°$. We choose $Ba_3Cd_2Sb_4$ as an example to illustrate the structure, as shown in Fig. 1(a). Its structure can be viewed as made of Ba^{2+} cations and $[Cd_2Sb_4]$ double chains that are interconnected through Sb–Sb bonds to form 2D $[Cd_2Sb_4]^{6-}$ layers.[22] As shown in Fig. 1(b), this space group has inversion symmetry P, two-fold rotation symmetry C_2, and mirror symmetry $M_{1\bar{1}0}$ as labeled in the Brillouin zone which is defined by the primitive unit cell of $Ba_3Cd_2Sb_4$. It should be noted that the reason for using the primitive unit cell here is that the band structure measured by ARPES is determined by the smallest repeating unit of the lattice, and it is also more convenient to clarify the topological properties. According to the first-principles calculations in Ref. [15], the conduction and valence bands with opposite parities are inverted at both the V and M points and the band crossing points form two quasi-1D nodal lines along V–M under the protection of mirror symmetry $M_{1\bar{1}0}$. With the spin-orbital coupling (SOC) considered, the quasi-1D nodal lines [red curved lines in Fig. 1(b)] are also gaped, leaving a global "curved band gap", in which system the topological invariants $\mathbb{Z}_2$ can be well defined with time reversal symmetry and inversion symmetry preserved. According to the parity criterion proposed by Fu and Kane,[6] $Ba_3Cd_2Sb_4$ was predicted to be a WTI with $\mathbb{Z}_2 = (0;110)$.[15]

The single crystals of $Ba_3Cd_2Sb_4$ were grown by the flux method, as described in Ref. [22]. Firstly, barium ingot, cadmium and antimony particle were put together with plumbum in an alumina crucible and sealed into a quartz tube with the ratio of Ba : Cd : Sb : Pb = 3.5 : 2 : 4 : 20. The tube was heated to 960 ℃ at a rate of 60 ℃/h and held for 10 h, then cooled to 500 ℃ at 1.5 ℃/h. The flux was removed by centrifugation. The atomic composition of the obtained single crystals was checked to be Ba : Cd : Sb = 3 : 2 : 4 by energy dispersive x-ray spectroscopy (Oxford X-Max 50). The single crystal x-ray diffraction (XRD) patterns and powder XRD patterns in Figs. 1(c) and 1(d) were collected with a Bruker D8 Advance x-ray diffractometer using Cu K_α radiation. The inset of Fig. 1(c) exhibits a picture of the typical grown $Ba_3Cd_2Sb_4$ single crystal with (110) surface. The powder XRD pattern, as shown in Fig. 1(d), can be well indexed to the structure of $Ba_3Cd_2Sb_4$ with space group $C2/m$.

The existence of an even number of topological SSs on a specific surface is the most direct evidence for a WTI state. For this purpose, we performed SSs calculations on the (110) and (010) plane to study the SSs distributions. The surface Brillouin zone definitions and projection directions of (110) and (010) planes are labeled in Fig. 1(b). The projection of bulk and surface bands on (110) dark surface is shown in Fig. 2(a), on the high symmetry point $\bar{V}(\bar{M})$ which is the projection of the bulk V and M point. It seems that there is a Dirac SS at the energy position of

−0.1 eV. We symmetrize the part of the purple dotted box in Fig. 2(a) and zoom in to Fig. 2(b). It seems that both branches of the SS originate from the conduction bands, and it is more clear when surface additional on-site energy is set to 0.1 eV in Fig. 2(c), which can raise the SS about 0.1 eV. Therefore, the SS on the (110) plane is a trivial SS. On the (010) plane, the bulk V and M points are projected to different positions in the surface Brillouin zone. It can be seen from Fig. 2(d) that there are metallic Dirac SSs connecting the conduction band and the valence band at both $\bar{V}$ and $\bar{M}$.[15] The presence of two topological SSs on the (010) plane is consistent with the weak topological invariant (110) for $Ba_3Cd_2Sb_4$.

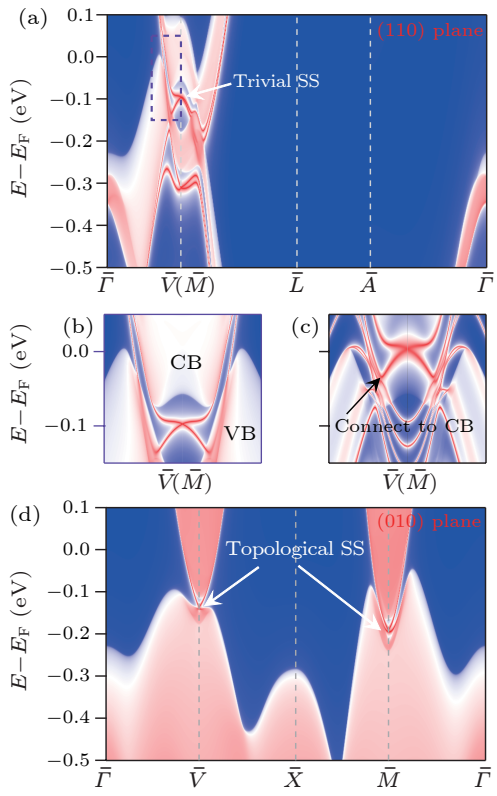

Fig. 2. (a) Calculated band dispersions of trivial SSs and projected bulk states on the (110) plane. (b) Zoom in of the purple dash box in (a). (c) Zoom in of the purple dash box in (a) when surface additional onsite energy is set to 0.1 eV. (d) Calculated band dispersions of topological SSs and projected bulk states on the (010) plane.

To further examine the theoretical prediction of the nontrivial topological phase in $Ba_3Cd_2Sb_4$, we have carried out systematical synchrotron-ARPES measurements on the (110) natural cleavage surface of $Ba_3Cd_2Sb_4$ single crystals. The orientation of the (110) plane in the crystal lattice and the corresponding surface Brillouin zone in the momentum space are shown in the red shaded areas in Figs. 1(a) and 1(b), respectively. ARPES measurements were performed at Beamline 7.0.2 (MAESTRO) at the Advanced Light Source and Beamline 09U (Dreamline) at the Shanghai Synchrotron Radiation Facility. Samples were cleaved and measured under ultrahigh vacuum better than 1×10^{-10} Torr. The overall energy and angular resolutions were better than 20 meV and 0.2°, respectively. Although the direct observation for the existence of the topological SSs is elusive since the cleaving surface is (110), which is a "dark surface" for the WTI. The V and M points where bulk band inversion happens are projected to the same point in the (110) surface Brillouin zone, which leads to the cancelation of two topological SSs. Spectroscopic evidence for WTI can be provided by ascertaining the bulk band structure and whether the band inversions occur at both of the V and M points on this "dark surface".

Figure 3(c) shows the in-plane FS measured with photon energy $h\nu = 115$ eV, there are small ellipses existing at the two boundaries of the surface Brillouin zone, which are the projections of the V and M points in the bulk Brillouin zone. The in-plane FS is perfectly reproduced by our HSE06 SSs calculations as shown in Fig. 3(a). The cleavage surface can also be confirmed to (110) according to the periodicity of the in-plane FS. As for the direction perpendicular to the cleaving surface (110), the calculated out-of-plane FS in Fig. 3(b) exhibits quasi-2D stick-shaped FS extending along V–M. We determine momentum locations along this direction by photon energy dependent ARPES measurements. The experimentally measured out-of-plane FS as shown in Fig. 3(d) is almost exactly the same as the theoretical calculations. This quasi-2D stick-shaped FS suggest that there is no significant change in the shape of the FS along this direction within the momentum resolution. Due to the finite mean free path of the photoelectrons, tiny changes in the shape of FS along the direction perpendicular to cleaving surface cannot be resolved by photon energy dependent ARPES measurements. The correspondence between the momentum positions of high-symmetry points and the photon energy can be determined according to photon energy dependence of the valence band dispersion. Figure 3(e) shows intensity plots of the ARPES data along the red and blue dashed line in Fig. 3(d), showing photon energy dependence of the valence band. Due to the potential influence of the matrix element effect, a noticeable dispersion can be observed only in the range 90–110 eV. It can be clearly seen that the band contributed by the dip of the M-shaped valence band is the lowest around 93 eV, and the highest around 105 eV in cut 1 and the opposite in cut 2. According to the calculated bulk band dispersions, the dispersion along V–M is very weak,[15] which is also conducive to the simultaneous occurrence of band inversions at the V point and the M point. It can still be distinguished that the energy is the lowest at the M point and the highest at the V point. Then we can determine the corresponding relationship between the position of the high symmetry point and the photon energy. We can find that the M point and the V point appear almost symmetrically under the same photon energy, which is consistent with the geometric structure of the Brillouin zone. This also proves the accuracy of our determination of the k-space position along the direction perpendicular to the surface. It is worth mentioning that it is still difficult for us to completely rule out the influence of "k_z broadening" effects, perhaps further soft x-ray ARPES measurements or ARPES measurements on different plane will help.

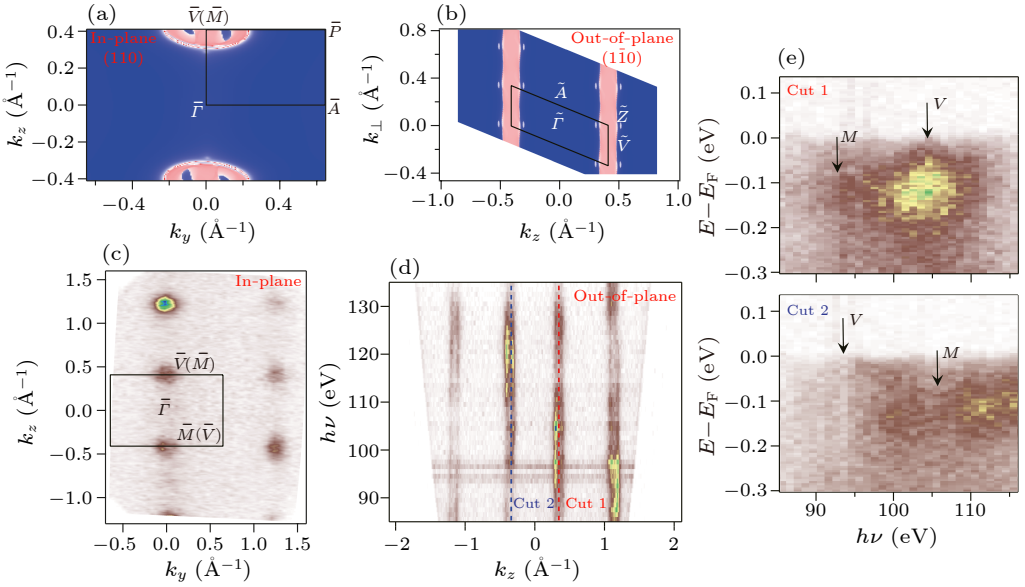

Fig. 3. Calculated Fermi surfaces of (110) plane (a) and (1$\bar{1}$0) plane (b). (c) ARPES intensity plots at E_F recorded on the (110) plane. (d) Intensity plot of the ARPES data at E_F collected in a range of photon energies from 85 to 135 eV on the (110) plane. (e) Intensity plots of the ARPES data along the red and blue dashed line in (d), showing photon energy dependence of the valence band.

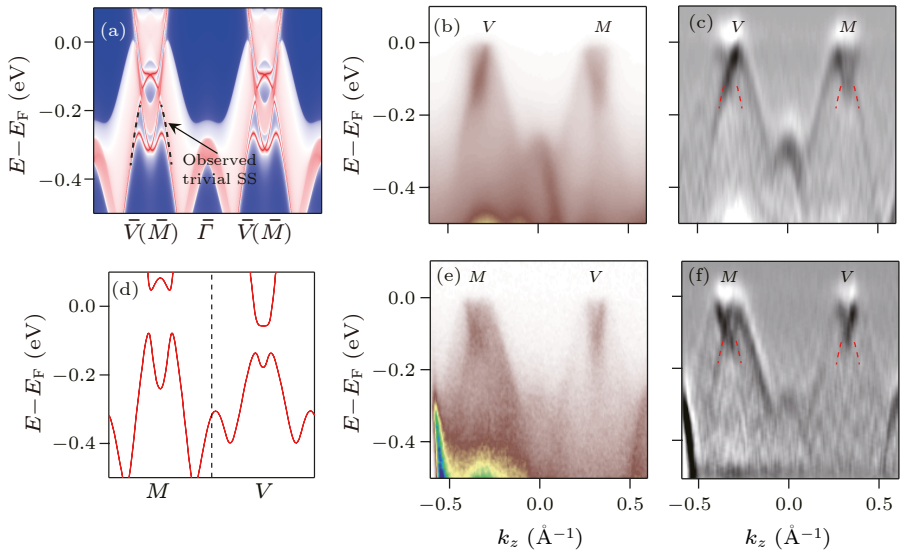

Fig. 4. (a) Calculated band dispersions of trivial SSs and projected bulk states along high symmetry lines on the (110) plane. Intensity plots of the ARPES data along V–M (b) and M–V (e). [(c), (f)] Two-dimensional derivative intensity plot of the data in (b) and (e). The dashed lines are guide to eyes of the trivial SS band dispersions. (d) Calculated bulk band dispersions along high symmetry lines M–V.

Figures 4(b) and 4(e) show the ARPES measured band structure near the V and M points with the photon energies of 93 eV and 105 eV, one of them is that the M point is in the positive direction and the V point is in the negative direction, and the other is the opposite. Two M-shaped valence band can be clearly seen near the Fermi level at both the V and M points, the Fermi level is near the band gap caused by SOC, which is a typical spectroscopic characteristic of band inversion. The band dispersions can be seen more clearly from the second derivative results of the ARPES intensity plots in Figs. 4(c) and 4(f), which are generally consistent with the calculated bulk band dispersion in Fig. 4(d). In addition, we identify an extra hole-like band slightly lower than the M-shaped valence band. As its dispersion is perfectly reproduced by our SSs calculations as shown in Fig. 4(a), we attribute it to a trivial SS on (110) plane. We find that the degree of band inversion at the V point is weaker than that at the M point, which is manifested by the depth of the dip in the middle of the M-shaped valence band with the trivial surface states as reference. The characteristics of these two band inversions are fully in line with the expectations of our

theoretical calculations. Further comparing the calculated and experimental observed dispersion of the bulk and the surface states, we find a modest downshift of chemical potential that leads to the computationally unexpected finite spectrum intensity contributed by the valence band at the Fermi level and the energetic discrepancy between the calculated and experimental observed trivial surface states. The downward shift in chemical potential may be due to defects in crystal growth or the presence of surface potential. On this topologically dark surface, the other indirect signals for the existence of topological SS such as the quasi-1D edge states can be measured by future scanning tunneling microscope experiment on step edges.[23,24]

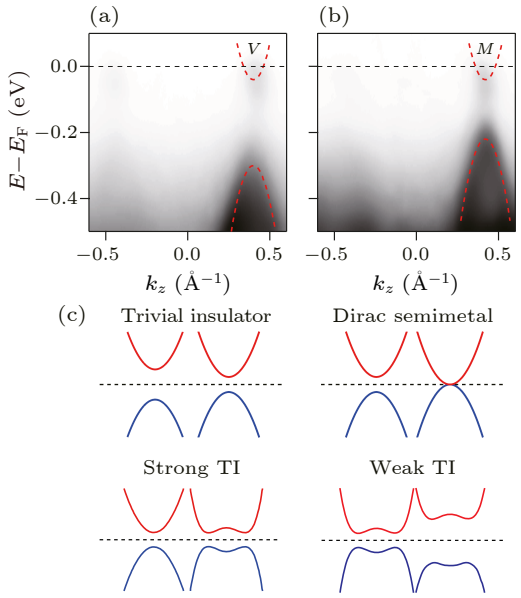

Fig. 5. ARPES intensity plots at the V point (a) and the M point (b) of $Ba_3Cd_2As_4$. (c) A schematic diagram of topological phase transition process from trivial semiconductor to WTI with the gradual enhancement of the degree of orbital splitting.

To further systematically study the band structure and topological properties of this family of materials. We have carried out synchrotron-ARPES measurements on the (110) cleavage surface of $Ba_3Cd_2As_4$ single crystal, which has a similar crystal and band structure to $Ba_3Cd_2Sb_4$, except a much smaller degree of orbital splitting and SOC compared to $Ba_3Cd_2Sb_4$.[15] Figures 5(a) and 5(b) show the band structure near the V and M points, respectively. It is clear that there is a positive band gap between the conduction and valence bands in both the V and M points, no band inversion occurs, which means that this material is a trivial semiconductor. The gap sizes at the V and M points are about 300 meV and 230 meV, respectively.

The topological protected dissipationless SS can be better practical utilized by artificially manipulation of the topological phase. Figure 5(c) is a schematic diagram for the topological phase transition process from trivial semiconductor to WTI with the gradual increase in the number of band inversions. $Ba_3Cd_2As_4$ and $Ba_3Cd_2Sb_4$ are located at the two endpoints of this phase transition process. A continuously topological phase transition can be induced by chemical doping or external stressing. For instance, applying compressive strain to $Ba_3Cd_2As_4$ can gradually enhance the degree of orbital splitting and lead to the occurrence of band inversions, and then sequentially realize the Dirac semi-metallic, strong TI, and WTI states.[15] The easily tunable topological properties make this family of materials greatly promising for applications.

In summary, by first-principles calculations and ARPES experiments, we have revealed the electronic structure of the (110) dark surface of the WTI candidate $Ba_3Cd_2Sb_4$ and trivial semiconductor $Ba_3Cd_2As_4$. All the experimental results can be perfect reproduced by our first-principles calculations. The existence of two Dirac SSs on specific side surfaces and the observed two band inversions in the Brillouin zone give strong evidence to prove that the $Ba_3Cd_2Sb_4$ is a WTI. The spectroscopic characterization of this Zintl $Ba_3Cd_2N_4$ (N = As and Sb) family materials will facilitate applications of their novel topological properties.

Calculation Method. The first-principles calculations are carried out with the Vienna *ab initio* simulation package (VASP).[25,26] The exchange-correlation potential is treated using the generalized gradient approximation (GGA) parametrized by Perdew, Burke, and Ernzerhof (PBE).[27] According to the previous work,[15] the calculated band structures with HSE06 hybrid functional[28] are consistent with the ARPES measurement, so the HSE06 hybrid functional is applied in all calculations. The cutoff energy is set to 450 eV and the Brillouin zone (BZ) is sampled with $4 \times 4 \times 4$ Monkhorst–Pack k-point mesh in the self-consistent calculation. Then, the bulk bands are calculated based on the self-consistent charge density by VASP. The calculation of surface states contains two steps. The first step is building the Wannier tight-binding Hamiltonian using VASP and WANNIER90 software.[29,30] The s orbits of Cd atoms and the p orbits of Sb atoms are chosen to construct the localized Wannier functions, and the Wannier tight-binding Hamiltonian and Wannier band structures are calculated. Only if the Wannier band structures fit well with the band structures obtained by VASP, the Wannier tight-binding Hamiltonian is correct. The second step is calculating the surface states from the Wannier tight-binding Hamiltonian using the open-source code WANNIERTOOLS.[31] The surface orientation is set according to the experimental measurement, and surface states spectra are calculated by the Green function method.

Acknowledgments. This work was supported by the National Key R&D Program of China (Grant Nos. 2022YFA1403800, 2018YFA0305700, and 2019YFA0308602), the Chinese Academy of Sciences (Grant Nos. QYZDB-SSW-SLH043, XDB33000000, and XDB28000000), the National Natural Science Foundation of China (Grant Nos. U22A600018, U1832202, 12074425, 11874422, 11925408, 11921004, and 12188101), the Informatization Plan of Chinese Academy of Sciences (Grant

No. CAS-WX2021SF-0102), and the Synergetic Extreme Condition User Facility (SECUF)

References

[1] Hasan M Z and Kane C L 2010 *Rev. Mod. Phys.* **82** 3045
[2] Qi X L and Zhang S C 2011 *Rev. Mod. Phys.* **83** 1057
[3] Bernevig B A, Hughes T L, and Zhang S C 2006 *Science* **314** 1757
[4] Konig M, Wiedmann S, Brune C *et al.* 2007 *Science* **318** 766
[5] Zhang P, Noguchi R, Kuroda K *et al.* 2021 *Nat. Commun.* **12** 406
[6] Fu L and Kane C L 2007 *Phys. Rev. B* **76** 045302
[7] Fu L, Kane C L, and Mele E J 2007 *Phys. Rev. Lett.* **98** 106803
[8] Yan B H, Müchler L, and Felser C 2012 *Phys. Rev. Lett.* **109** 116406
[9] Rasche B, Isaeva A, Ruck M *et al.* 2013 *Nat. Mater.* **12** 422
[10] Weng H, Dai X, and Fang Z 2014 *Phys. Rev. X* **4** 011002
[11] Tang P Z, Yan B H, Cao W D *et al.* 2014 *Phys. Rev. B* **89** 041409
[12] Liu C C, Zhou J J, Yao Y, and Zhang F 2016 *Phys. Rev. Lett.* **116** 066801
[13] Eschbach M, Lanius M, Niu C *et al.* 2017 *Nat. Commun.* **8** 14976
[14] Lee K, Lange G F, Wang L L *et al.* 2021 *Nat. Commun.* **12** 1855
[15] Zhang T, Yue C, Zhang T *et al.* 2019 *Phys. Rev. Res.* **1** 012001(R)
[16] Huang J W, Li S, Yoon C *et al.* 2021 *Phys. Rev. X* **11** 031042
[17] Xu L X, Xia Y Y Y, Liu S *et al.* 2021 *Phys. Rev. B* **103** L201109
[18] Wan Q, Yang T Y, Li S *et al.* 2021 *Phys. Rev. B* **103** 165107
[19] Lin C, Ochi M, Noguchi R *et al.* 2021 *Nat. Mater.* **20** 1093
[20] Pauly C, Rasche B, Koepernik K *et al.* 2016 *ACS Nano* **10 4** 3995
[21] Noguchi R, Takahashi T, Kuroda K *et al.* 2019 *Nature* **566** 518
[22] Saparov B, Xia S Q, and Bobev S 2008 *Inorg. Chem.* **47** 11237
[23] Liu R Z, Huang X, Zhao L X *et al.* 2019 *Chin. Phys. Lett.* **36** 117301
[24] Liu S, Nie S M, Qi Y P *et al.* 2021 *Chin. Phys. Lett.* **38** 077302
[25] Kresse G and Furthmüller J 1996 *Comput. Mater. Sci.* **6** 15
[26] Kresse G and Furthmüller J 1996 *Phys. Rev. B* **54** 11169
[27] Perdew J P, Burke K, and Ernzerhof M 1996 *Phys. Rev. Lett.* **77** 3865
[28] Heyd J, Scuseria G E, and Ernzerhof M 2003 *J. Chem. Phys.* **118** 8207
[29] Mostofi A A, Yates J R, Lee Y S *et al.* 2008 *Comput. Phys. Commun.* **178** 685
[30] Marzari N, Mostofi A A, Yates J R *et al.* 2012 *Rev. Mod. Phys.* **84** 1419
[31] Wu Q S, Zhang S N, Song H F *et al.* 2018 *Comput. Phys. Commun.* **224** 405